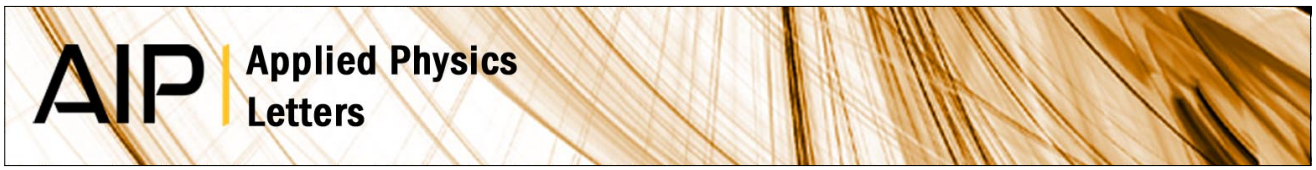

Confinement effects on the low temperature magnetic structure of MnP nanocrystals

A. de Andrés, R. Ramírez-Jiménez, M. García-Hernández, S. Lambert-Milot, and R. A. Masut

Citation: Appl. Phys. Lett. **99**, 182506 (2011); doi: 10.1063/1.3658393
View online: http://dx.doi.org/10.1063/1.3658393
View Table of Contents: http://apl.aip.org/resource/1/APPLAB/v99/i18
Published by the American Institute of Physics.

Confinement effects on the low temperature magnetic structure of MnP nanocrystals

A. de Andrés,[1,a)] R. Ramírez-Jiménez,[2] M. García-Hernández,[1] S. Lambert-Milot,[3] and R. A. Masut[3]
[1]*Instituto de Ciencia de Materiales de Madrid, CSIC, Cantoblanco, 28049 Madrid, Spain*
[2]*Departamento de Física, Escuela Politécnica Superior, Universidad Carlos III de Madrid, Avenida Universidad 30, 28911 Madrid, Spain*
[3]*Regroupement québécois sur les matériaux de pointe (RQMP) and Département de génie physique, École Polytechnique de Montréal, CP 6079 Succ. Centre-ville, Montreal, Quebec H3C 3A7, Canada*

(Received 20 July 2011; accepted 13 October 2011; published online 2 November 2011)

The low temperature magnetic properties of MnP nanocrystals (15-40 nm), both in GaP:MnP epilayers and MnP films, are significantly different compared to bulk and cannot apparently be explained by differences in the structure. A simple model of localized spins is used to describe the magnetic screw structure confined to nanocrystals. The results indicate that the observed magnetic behaviour is related to the nanometric size and to changes in the coupling constants most probably localized at an external grain shell. The nucleation of helical regions at the surface of the ferromagnetic grains is proposed as a possible mechanism for the reversal of the magnetization. © *2011 American Institute of Physics*. [doi:10.1063/1.3658393]

Magnetic semiconductors with high ferromagnetic transition temperatures (T_C) and spin polarized carriers are the paradigm for spintronics, however, so far, III-V based materials present low T_C and metal transition doped oxides, with high T_C's, are still not well controlled, many times with non homogeneous dopant distribution forming nanosized metastable phases in the matrix.[1–3] On the other hand, Mn-based submicron ferromagnets embedded in III-V semiconductor host layers offer interesting properties for magneto-electronic devices and can in principle be tailored to exhibit room-temperature ferromagnetic behaviour as well as giant magneto-optical Kerr and Faraday effects.[1,4,5] Therefore, in order to obtain promising functionalities and devices, we focussed on the combination of MnP, a RT ferromagnet, and GaP, a wide indirect gap semiconductor, which are nearly lattice-matched to Si. Here, we present and discuss the magnetic properties of MnP nanocrystals in two different situations: embedded in GaP epilayers and as polycrystalline thin films, both grown by metal organic vapour phase epitaxy (MOVPE) on GaP (001). Previous detailed structural characterizations established that MnP nanocrystals (15–20 nm in diameter) are embedded in GaP:Mn epilayers that are semi-coherent with the substrate.[6] The grains of the studied MnP film have around 40 nm and lattice parameters within 0.2% of bulk MnP.[7] Since the local structure and symmetry of Mn in MnP nanocrystals are found to be similar to those of bulk crystals and strain effects seem hardly compatible with the reported variations of both transition temperatures T_C and T_N,[7] it becomes important to determine what is at the origin of the markedly different magnetic behavior of the nanocrystals, particularly at low temperatures. A simple model including ferro- (J_1) and antiferro-magnetic (AFM) (J_2) interactions is further developed here to evaluate the effects of nanometric size on the magnetic structure of MnP.

Bulk MnP crystallizes in the Pbnm space group ($a = 5.918$ Å $> b = 5.258$ Å $> c = 3.172$ Å (Ref. 8)]) and presents a strong biaxial magneto-crystalline anisotropy with its longer axis (a) as the harder magnetic axis, and the shorter (c), the softer. MnP is ferromagnetic below $T_C = 291.5$ K, hellimagnetic (screw) below $T_N = 47$ K and shows field induced transitions.[9,10] At 4 K, a full rotation of the magnetic moment is completed each $9a$ (about 5 nm).[11] GaP:MnP films, around 300 nm thick, were grown on GaP(001) substrates in a low-pressure cold-wall MOVPE reactor[7] at 650 °C. MnP films were grown under similar conditions, also on GaP (001). The MnP powder was commercially obtained from Alfa Aesar, whose average grain size is 150 μm. The magnetic characterization was achieved as a function of temperature (2–350 K) and magnetic field (up to 5T) with a superconducting quantum interference device magnetometer from Quantum Design.

Fig. 1 shows the large shift to higher temperatures of T_N (from 47 K for bulk to 82 K for MnP:GaP) while T_C changes slightly (see derivatives in Fig. 1(c)). Also, while the field cooled (FC) magnetization in the screw phase is almost zero in bulk MnP, in MnP film, and in nanocrystals, the magnetization remains significant. Figs. 1(d) and 1(e) evidence the similarities between the films. Both show high coercive fields (H_C) in the screw and collinear ferromagnetic phases as well as high remanence in contrast to the bulk ($H_C \simeq 0$ and no remanence, in powder or single crystal[7,9]).

To study the effect of the nanocrystals finite size, we calculated the ground state magnetic structure for a slice of MnP with its finite length along the screw axis a (size $= Na/2$, where $N =$ number of planes perpendicular to a) using the Hamiltonian and parameters from Ref. 13. A 1D model along the hard (a) axis can be justified because the major effect of confinement occurs along this axis, while confinement in the two perpendicular directions (b and c axes) is expected to be relevant on the smaller scale of the Mn-Mn distance (~0.3 nm) and, thus, can be ignored for the 15–40 nm clusters

[a)]Electronic mail: ada@icmm.csic.es.

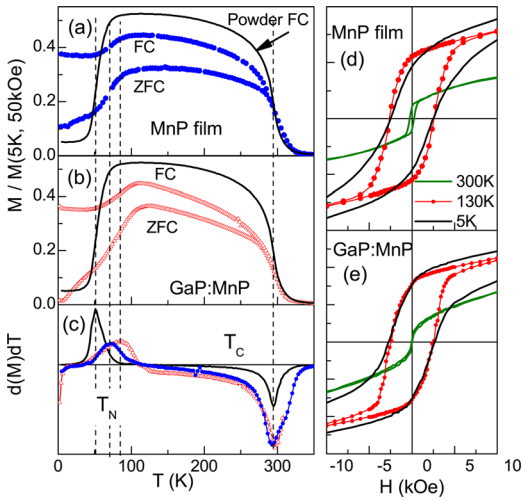

FIG. 1. (Color online) FC and ZFC Magnetizations measured at 1 kOe, normalized to the values at 5 K and 50 kOe, of (a) MnP film, (b) GaP:MnP, and for MnP powder (black line). (c) Magnetization derivatives showing the two magnetic transitions. Magnetization cycles at 5 K, 130 K, and 300 K of (d) MnP film and (e) GaP:MnP epilayer.

we are considering here. The magnetic ground state of bulk MnP was calculated by considering localized spins on Mn, which are coupled FM within the planes perpendicular to the hard a axis. The different planes have equivalent spins S_n whose directions are fitted to minimize the magnetic energy. The exchange coupling of each layer with its nearest neighbour is FM (J_1), while it is AFM with its next nearest layer (J_2).[12] In the absence of anisotropy, the ratio J_2/J_1 determines whether the ground state is FM or screw (if $J_2/J_1 > 1/4$). The ground state for an infinite MnP crystal is the screw phase with an angle between the magnetic moments of two successive planes $\alpha = 21°$,[13] in agreement with experimental results.[11]

The helical structure varies with the crystal size ($Na/2$), as determined by energy minimization. Fig. 2(a) presents the evolution of α along the a direction for two grain sizes (N = 60, N = 25), showing the drastic reduction of α for the 5-6 planes near each surface. Therefore, the deviation from the uniform helical bulk structure is more important as the size is reduced. Fig. 2(b) represents the magnetic moments of the planes for two grains with similar number of planes N = 28 and N = 32. The total resulting moment is different

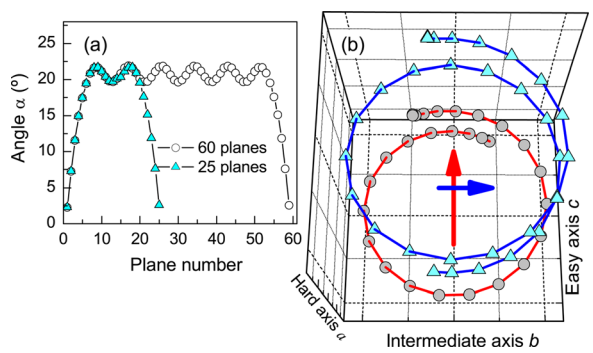

FIG. 2. (Color online) (a) Calculated angles between the magnetic moments of two successive planes (α) in grains with N = 25 (7.4 nm) and 60 (18 nm) along their hard a axis. (b) 3D representations of the ends of the magnetic moment vectors for each plane in two cases N = 28 (circles) and N = 32 (triangles). The arrows indicate the directions of the resulting moments of the whole grain (vertical N = 28 (8.3 nm) and horizontal N = 32 (9.5 nm)).

from zero (contrary to what occurs for an infinite screw phase) and switches from the easy axis, c, to the intermediate axis, b, depending on the size of the nanocrystals, due to the magnetic anisotropy. Fig. 3 represents the total magnetization (normalized to the fully ferromagnetic value) versus the number of planes along the hard direction. Both components, in the bc plane, are plotted in the upper panel. The direction of the whole grain magnetization switches between b and c axes as the size increases. The range of sizes of the MnP nanocrystals in GaP and grains in the MnP film is indicated with horizontal arrows in Fig. 3(b).

These calculations also indicate that the magnetization of nanocrystals is finite and significant (between 5% and 10% of that of a collinear ferromagnetic magnetization) and explain the measured FC and zero field cooled (ZFC) magnetization curves; after ZFC, the different grains have a net magnetic moment with a random distribution along both senses of b or c axes so that the measured moment is almost zero (Fig. 1, ZFC curves). When the samples are FC, the moments align with the applied field (Fig. 1, FC) and result in a non-zero magnetic moment in the bc plane (Fig. 3). FC and ZFC curves differ up to about T_C due to the high coercive fields of the samples (2–2.7 kOe) compared to the applied field, 1 kOe. The calculated net moment per plane increases as the crystal size decreases (Fig. 3) indicating that the ferromagnetic ground state is favoured in nanocrystals. In fact, the suppression of T_N has been observed in synthesized orthorhombic MnP nanorods with their growth direction along the b axis and a small diameter (~5 nm),[14] which corresponds to an extreme confinement of the screw structure along the hard axis a. In the MnP embedded clusters and polycrystalline films reported here, with larger crystal sizes (15–40 nm), T_N is observed to increase significantly.

The reported hydrostatic or uniaxial strain effects in bulk MnP,[15,16] do not offer a straightforward explanation for the observed variations of T_C and T_N.[7] However, it is reasonable to suppose that J_1 and J_2 may vary in nanocrystals due to the important weight of the surface Mn compared to bulk. Within this framework, we have estimated the dependence of both transition temperatures on the strength of both coupling

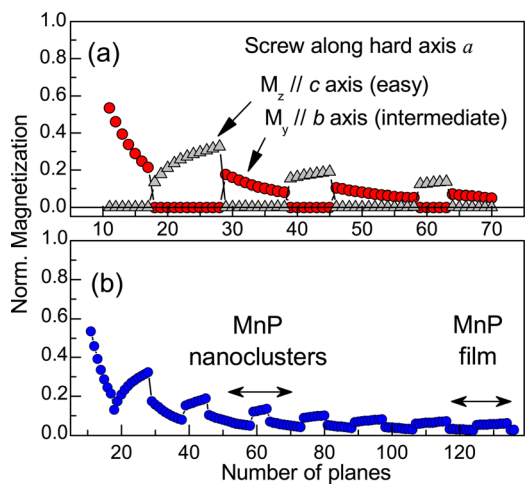

FIG. 3. (Color online) Magnetization normalized to the fully ferromagnetic value vs. the number of planes in the grain (a) along b direction (red circles) and along c (grey triangles). (b) Modulus of the normalized magnetization. N = 10 corresponds to ca. 3 nm.

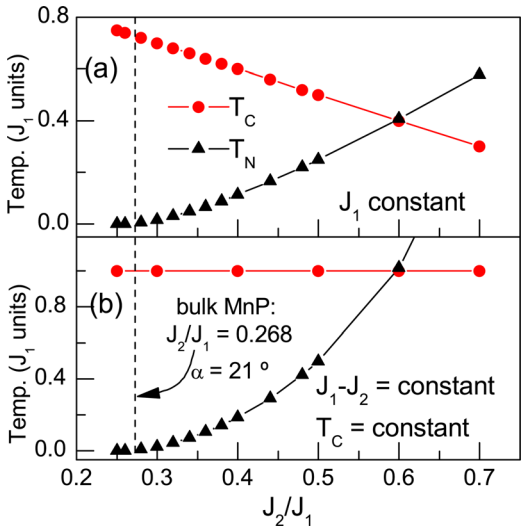

FIG. 4. (Color online) Evolution of T_C and T_N, with the absolute value of J_2/J_1 (J_1 ferro- and J_2 antiferro-magnetic coupling constants) in bulk MnP for different conditions: (a) J_1 = constant and (b) ($J_1 - J_2$) = constant.

parameters. In an infinite crystal, the minimization of the energy per plane $E = -J_1\cos(\alpha) + J_2\cos(2\alpha)$ (taking $J_2 > 0$) yields $\cos(\alpha) = J_1/(4J_2)$.[12] Thus, the screw phase ($\alpha \neq 0$) occurs for $J_2/J_1 > 1/4$ with an energy $E_{min} = -J_1(\gamma + 1/8\gamma)$, where $\gamma = J_2/J_1$, which deepens as J_2/J_1 increases. Since the energy of the ferromagnetic state ($\alpha = 0$) is $E_{FM} = J_2 - J_1$, T_C is directly related to $J_2 - J_1$, whereas T_N is related to the difference: $E_{min} - E_{FM}$. Even if the model is oversimplified, the predicted tendencies for the transition temperatures of both the FM and screw phases are expected to be reliable.

Fig. 4 presents the evolution of T_C and T_N as a function of the parameters J_1 and J_2. In the upper panel, the J_2/J_1 ratio increases while J_1 is fixed, therefore only J_2 increases. In this case, close to the J_2/J_1 bulk value for MnP (0.268), T_C and T_N vary in opposite directions; T_N varying more slowly, as it occurs when applying hydrostatic or uniaxial pressures. For $J_2/J_1 \leq 1/4$, the system becomes ferromagnetic and T_N as well as α are zero. When ($J_1 - J_2$) is maintained constant and, therefore, T_C is constant (lower panel) by increasing the ratio J_2/J_1, T_N increases. Therefore, the combination of a constant T_C and an increase of T_N observed for the films with grains in the nanometric range can be explained within this model by an increase of both the ferromagnetic and antiferromagnetic couplings, most probably due to the different environment of Mn at the outmost shell of the grains.

The observed coercive fields are high (above 2kOe) but lower than the field corresponding to a single domain coherent rotation with the anisotropy constants of bulk MnP.[7] The discussed changes in the magnetic structure and magnetic interactions are also providing a lower energy mechanism for the magnetization rotation. The nucleation of helical regions at the grain surface, which is favoured by the antiferromagnetic coupling compared to an ordinary ferromagnetic system, may be propagated to the grain requiring a much lower energy, i.e., lower coercive fields, than bulk values of a coherent reversal.

From this model, one can conclude that the observed low temperature magnetism of MnP nanocrystals is related to their nanometric size and to surface effects. Model simulations show that the screw magnetic structure is altered by the finite size of the grains giving rise to a net ferromagnetic moment arising from the outmost five or six Mn planes. Since the structure inside the grains seems unchanged compared to bulk while the surface is subject to strain and disorder, it is reasonable to locate the major changes in a shell of a few atomic planes with different magnetic interactions, J_1 and J_2, which explains the observed large increase of T_N while maintaining T_C almost unchanged. Therefore, local changes in ferromagnetic and antiferromagnetic coupling constants at the surface of the grains, combined with effects in the magnetic structure related to the nanometric size, are postulated at the origin of the differences in the low temperature magnetic behaviour of MnP nanocrystals as compared to powder or single crystals.

We acknowledge the financial support from the Spanish Ministry MICINN (MAT2009-08786, MAT-2008-06517, and CSD2009-00013), from "Comunidad de Madrid" (No. S2009/MAT-1756), and by the Natural Sciences and Engineering Research Council of Canada (NSERC), the infrastructure support of the RQMP (Québec), and the technical assistance of Joël Bouchard.

[1]T. Dietl, Nature Mater. **9**, 965 (2010).
[2]J. M. D. Coey, M. Venkatesan, and C. B. Fitzgerald, Nature Mater. **4**, 173 (2005).
[3]A. Espinosa, M. García-Hernández, N. Menéndez, C. Prieto, and A. de Andrés, Phys. Rev. B **81**, 064419 (2010).
[4]G. A. Prinz, Science **282**, 1660 (1998).
[5]A. Gabriel Monette, C. Lacroix, S. Lambert-Milot, V. Boucher, D. Ménard, and S. Francoeur, J. Appl. Phys. **107**, 09A949 (2010).
[6]S. Lambert-Milot, C. Lacroix, D. Ménard, R. A. Masut, P. Desjardins, M. García-Hernández, and A. de Andrés, J. Appl. Phys. **104**, 083501 (2009).
[7]A. de Andrés, A. Espinosa, C. Prieto, M. García-Hernández, R. Ramírez-Jiménez, S. Lambert-Milot, and R. A. Masut. J. Appl. Phys. **109**, 113910 (2011).
[8]S. Rundqvist and P. C. Nawapong, Acta Chem. Scand. **19**, 1006 (1965).
[9]E. E. Huber and D. H. Ridgley, Phys. Rev. **135**, A1030 (1964).
[10]M. S. Reis, R. M. Rubinger, N. A. Sobolev, M. A. Valente, K. Yamada, K. Sato, Y. Todate, A. Bouravleuv, P. J. von Ranke, and S. Gama, Phys. Rev. B **77**, 104439 (2008).
[11]C. C. Becerra, H. J. Brumatto, and N. F. Oliveira, Phys. Rev. B **54**, 15997 (1996).
[12]An AFM constant (J_2) is negative, however here we take both J_1 and J_2 as positive, and explicitly incorporate the sign in the Hamiltonian.
[13]A. Zieba, M. Slota, and M. Kucharczyk, Phys. Rev. B **61**, 3435 (2000).
[14]K. A. Gregg, S. C. Perera, G. Lawes, S. Shinozaki, and S. L. Brock, Chem. Mater. **18**, 879 (2006).
[15]E. Hirahara, T. Suzuki, and Y. Matsumura, J. Appl. Phys. **39**, 713 (1968).
[16]E. Iwata, J. Sci. Hiroshima Univ., Ser. A-2 **33**, 1 (1969).